Droplet capture in a fiber array

Karl Cardin,[1] Christophe Josserand,[2] and Raúl Bayoán Cal[1,*]
[1]*Portland State University, Portland, Oregon 97201, USA*
[2]*Laboratoire d'Hydrodynamique (LadHyX), UMR 7646 CNRS-Ecole Polytechnique, IP Paris, 91128 Palaiseau CEDEX, France*

(Received 2 August 2022; accepted 15 February 2023; published 7 April 2023)

Droplets interacting with fiber arrays is ubiquitous in nature, textiles, microelectromechanical devices, and fog harvesting. The phenomena of droplet impact on an equidistant array of fibers is experimentally investigated. Drop tower tests are performed to characterize the droplet dynamics in the absence of the effects of gravity which could deform fibers and bias equilibrium configurations. Results show that contact line dissipation is largely responsible for arresting the droplet. Additionally, the penetration length is affected by fiber flexibility. A model is developed predicting the droplet penetration dynamics which shows good agreement with experiments.

DOI: 10.1103/PhysRevFluids.8.043601

I. INTRODUCTION

The interaction of droplets with slender structures is ubiquitous in both nature and technology. Nature has utilized fiber arrays for functions such as rejecting condensed water droplets from the legs of water striders using flexible setae to maintain flotation [1] and water collection by plants in arid environments [2–5]. Taking inspiration from nature, arrays of stretched fibers have been shown to effectively recover water from fog [6]. Understanding the interaction between capillary forces and the deformation of structures such as carbon nanotube carpets is important for the manufacturing of microelectromechanical devices [7]. The effects of structure, wettability, flexibility, for example, on the ability of a fiber structure to capture a droplet and the final equilibrium configuration of the droplet remain rich areas of research.

Drop impacts on horizontal fibers, where the droplet velocity is normal to the fiber axis, have recently received much attention while on-axis impacts have lagged behind. The critical velocity threshold between capture and fragmentation was quantified for inviscid droplets impacting a fixed fiber [8]. The critical velocity of capture increases for a droplet impacting an angled fiber [9]. Studies of drop impact on horizontal flexible fibers demonstrate that droplet capture efficiency can be increased by modifying the fiber flexibility [10,11]. Nasto *et al.* [12] used energy arguments to identify a variety of regimes for on-axis droplet impact on fiber arrays constructed from casting polydimethylsiloxane.

Insight into the equilibrium configurations of liquid bodies in fiber arrays is valuable for its relevance to many applications such as fog harvesting and textile manufacturing. Investigations have examined the equilibrium configuration of liquid bridging multiple fibers [13–19]. Princen [17] predicted the cross-sectional shape of liquid columns between various equidistant arrays of cylinders, neglecting gravity, for a range of contact angles. Protiere *et al.* [18] investigated the transition between column and attached droplet configurations for perfectly wetting drops between two rigid cylinders, finding dependence on the drop volume, cylinder radius, and cylinder spacing.

*Corresponding author: rcal@pdx.edu

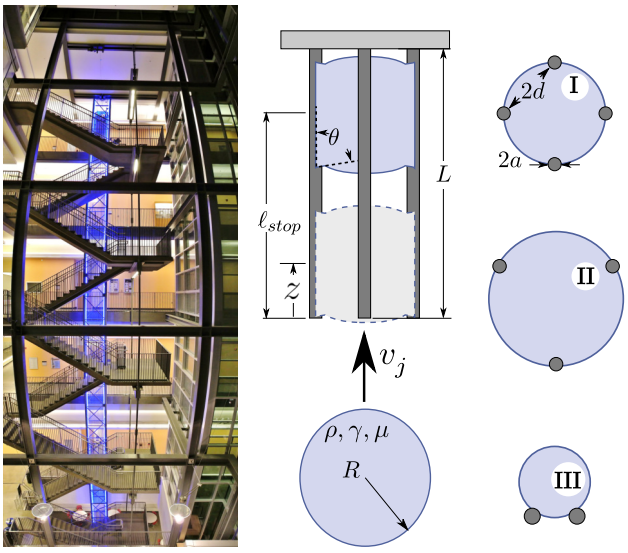

(a) (b)

FIG. 1. (a) Photo of the five-story Dryden Drop Tower at Portland State University. (b) Diagram of a droplet impacting a fiber array with relevant parameter shown and illustrations of relevant fiber array patterns: square (I), triangular (II), line (III).

Duprat *et al.* [13] showed that elasticity promoted droplet spreading between flexible fibers. The clustering of many fibers as they are withdrawn from a bath of wetting liquid has also been studied [19,20].

Previous studies of droplets traveling on fibers have focused on the viscocapillary systems. Such systems include droplets traveling along a conical fiber where the gradient in droplet curvature drives the motion while viscous dissipation resists the motion [21]. A similar case of a bubble traveling along a fiber submerged in a bath of liquid has also been investigated where the dynamics are dominated by buoyancy and viscous dissipation [22].

Here, a visco-inertial system of droplet penetration and capture in a fiber array is studied—a regime which is unique to mesoscale fibers [12]. Additionally, challenges of manufacturing and experimental imaging that an experiment with microliter droplets would encounter are circumvented. By utilizing the unique low-gravity environment of a drop tower, the fibers are free from gravity-induced deformations. Such experiments inform technologies such as water recovery from aerosols in space, which will be critical for long duration space travel. In addition to the relevance to low-gravity technologies, such experiments will help to disentangle the different contributions to terrestrial droplet penetration dynamics. In particular, droplet dynamics and equilibrium configurations will not be affected by the droplet and fiber weights. This paper is outlined as follows: The drop tower experimental apparatus is discussed, then data from a large drop tower test campaign is presented, and finally models are presented which predict the penetration length of a droplet into a fiber array.

II. METHODS

All experiments are performed at the Dryden Drop Tower (DDT) facility at Portland State University. The DDT is a safe, low-cost, high-rate facility located in the atrium of an engineering building on campus. An image of the tower is provided in Fig. 1(a). The experimental apparatus is mounted to an aluminum chassis, or 'drop rig', which hangs inside the drop tower drag shield before each drop. During a drop test, the rig and drag shield are released simultaneously and do not make

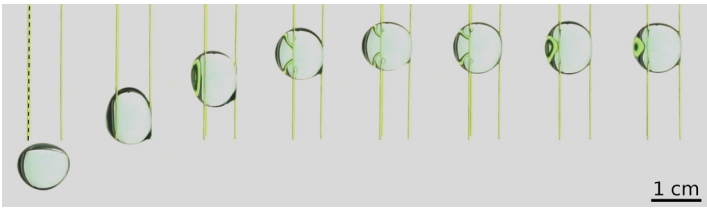

FIG. 2. Montage from a drop tower test showing a 0.25ml droplet entering a three-fiber array. The location of the third, not clearly visible fiber is depicted by the dashed line.

contact throughout the microgravity period of the drop tower test; because the rig is enclosed in the drag shield, the rig is largely protected from aerodynamic drag during free fall. The drag shield and experiment rig fall 22 m providing 2.1 s of relative low-gravity g $<10^{-4}g_0$. Additional DDT introduction details are provided by Wollman [23] and Cardin [24].

Figure 1(b) shows a diagram of the fiber impact experiment with relevant parameters indicated. Nylon monofilament fishing line or stainless steel rod of diameter $2a$, ranging from 0.2–1.6 mm, is used for the fibers. Nylon fibers are straightened by threading through glass capillaries with inner diameter $\sim 2a$ [25] and then placing in an oven at 50–100 °C for a minimum of 5 minutes. Straightened fibers of length L are attached in patterns with edge-to-edge distance $2d$ to a fixture plate which allows them to be accurately positioned, centered over the droplet at the beginning of the drop tower test. The static contact angle θ of the fibers is determined to be $\sim 60^\circ$ from inspecting the contact line of droplet in equilibrium during drop tower tests.

The drop jump mechanism [26] is used to generate impacting droplets. A concave superhydrophobic substrate is created by coating a concave lens with Glaco Mirror Coat (Soft 99). The resulting substrate has a static contact angle of 165 °. Before each drop tower test, a volume $(4/3)\pi R^3$ of fluid with density ρ, surface tension γ, and dynamic viscosity μ is deposited onto the superhydrophobic substrate using a syringe. Water with a small amount of dye added for visualization is used as the working fluid. The slight curvature of the superhydrophobic surface allows more accurate positioning of the droplet. At the beginning of the drop tower test, following the step reduction in gravity, the excess surface energy of the droplet is transferred into kinetic energy causing the droplet to travel away from the superhydrophobic substrate and towards the fiber array at the jump velocity v_j. During the drop tower test, the droplet impacts the fiber array, travels along the fibers, and either stops at a distance ℓ_{stop} or travels the full fiber length and impacts the fixturing plate. Additional details regarding the droplet jump mechanism are provided in Ref. [26].

All experiments are imaged at 120 fps with 1920 × 1080 pixel resolution using consumer-grade Panasonic cameras, model HC-WX970. A diffuse LED array is adopted to backlight the phenomena. Droplet velocities, droplet equilibrium positions, fibers deflections, etc., are extracted from video using image analysis software Fiji [27].

III. MODEL

Typical snapshots of the droplet impingement on the fibers (here, 3 fibers) are shown in Fig. 2 for illustration. There, the droplet penetrates into the fibers array, where it decelerates until it stops at a given length. It is important to emphasize here that, in the absence of gravity, the different forces that can explain the arrest of the droplet are the viscous, the capillary, and the elastic ones. However, since almost no fiber deformation at equilibrium is observed and that the capillary forces almost balance each other after the drop wets the fibers (there should be in fact a small difference between the advancing and receding contact angle, that can be neglected here), in the model below only the viscous dissipation is considered. Then, assuming simple droplet and meniscus geometries, a model is deduced where viscous dissipation is the main physical ingredient for the dynamics at first approximation. Viscous forces are proportional to the gradient of the velocity which are very

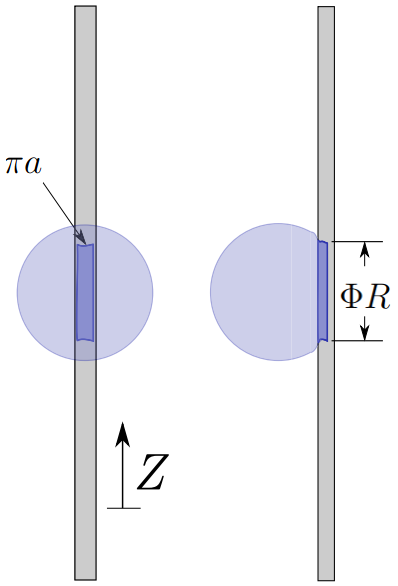

FIG. 3. Diagram showing the simplified contact region of a droplet attached to a single fiber. Such a contact region is assumed for each fiber.

high, close to the contact line, so that one can usually consider that the viscous dissipation can be decomposed in two distinct contributions, one coming from the velocity gradient in the bulk, the other from the motion of the contact lines along the fiber [28–30]. Therefore, to predict the penetration of the droplet into the fiber array, these two forms of viscous dissipation are considered, one which acts in the fluid bulk and the other along the droplet contact lines on the fibers. Near the moving contact line, the viscous force is given by [30]

$$\mathrm{F}_{cl} = \ell_{cl} \frac{3\mu \dot{z}}{\theta} \ln\left(\frac{\ell_M}{\ell_m}\right), \tag{1}$$

where z is the droplet center height (and thus $\dot{z}$ the vertical velocity of the droplet, see Fig. 1), and ℓ_M and ℓ_m are the macroscopic and microscopic cutoff sizes, respectively. We choose the characteristic distance between fibers for the macroscopic cutoff (take $\ell_M \sim 1$ mm) and the molecular size for the microscopic cutoff $\ell_m \sim 1$ Å, so that we take $\ln(\ell_M/\ell_m) \simeq 16$. Considering Fig. 3, the contact length ℓ_{cl} can be written as

$$\ell_{cl} = n_f 2(\pi a + \Phi R), \tag{2}$$

where Φ is a free parameter which accounts for the length of the contact line along the fiber. Additionally, a bulk viscous force $\mathrm{F}_{\mathrm{bulk}}$ is considered, resulting from the fluid between each set of nearest-neighbour fibers. The velocity gradient between two neighboring fibers is of the order $\dot{z}/d$, so dissipation is of the order $\mu \dot{z}/d$. This force to act over the contact area shown in Fig. 3 is considered. The bulk viscous force is therefore expressed as

$$\mathrm{F}_{\mathrm{bulk}} = A_c \mu \frac{\dot{z}}{d}, \tag{3}$$

defining A_c considering Fig. 3 as

$$A_c = n_f(\pi a \Phi R), \tag{4}$$

where n_f is the number of fibers that the drop encounters.

The relative magnitude of the two dissipation terms is

$$\frac{F_{cl}}{F_{\text{bulk}}} = \frac{\ell_{cl}}{A_c}\frac{3d}{\theta}\ln\left(\frac{\ell_M}{\ell_m}\right). \tag{5}$$

For the fiber arrays studied in this work, the contact line dissipation dominates $F_{cl}/F_{\text{bulk}} > 1$. For the fiber array geometries explored, $d/a > 1$, droplet wicking between fibers is expected to be minimal [17] and the droplets are expected to remain largely spherical, or in the 'drop' configuration [18].

For the forces at hand, Newton's law of dynamics can be written

$$\frac{d}{dt}(M\dot{z}) + F_{cl} + F_{\text{bulk}} = 0, \tag{6}$$

where M is the mass of the droplet. Substituting Eq. (1) and Eq. (3) into Eq. (6), letting

$$\zeta = \frac{1}{M}\left(\ell_{cl}\frac{3\mu}{\theta}\ln\left(\frac{\ell_M}{\ell_m}\right) + A_c\frac{\mu}{d}\right), \tag{7}$$

and using initial conditions $z(0) = 0$ and $v(0) = v_0$ yield the solution

$$z(t) = \frac{v_0}{\zeta}(1 - e^{-\zeta t}). \tag{8}$$

Since the liquid wets the fiber, the drop is somehow accelerated when entering the fiber array and a prediction of the initial velocity v_0 can be constructed using an energy argument. The droplet kinetic energy after entering the fiber array is thus $\varepsilon_{k,2} = \varepsilon_{k,1} + \varepsilon_\gamma$, where $\varepsilon_{k,1} = (1/2)Mv_j^2$ and ε_γ is the difference of the surface energy between the drop-fibers system before and after the penetration. In the view that this final kinetic energy corresponds to the initial velocity v_0 of the droplet to be considered in the model, it yields

$$v_0 = \sqrt{v_j^2 - \frac{2}{M}\varepsilon_\gamma}. \tag{9}$$

Due to the droplet remaining largely spherical, the change in surface energy can be estimated simply by neglecting the variation of the droplet surface so that only the wetted parts of the fibers $A_{S,G\to L}$ have to be considered leading to $\varepsilon_\gamma = A_{S,G\to L}(\gamma_{SG} - \gamma_{SL})$, where $A_{S,G\to L}$ is the fiber area that becomes covered by liquid, γ_{SL} is the solid/liquid surface tension, and γ_{SG} is the solid/gas surface free energy. The energy transformed to surface energy depends on the geometry of the fiber array. Using these assumptions and the Young equation $\gamma_{SL} - \gamma_{SG} = -\gamma\cos\theta =\sim -\frac{1}{2}\gamma$, the surface energy becomes

$$\varepsilon_\gamma = -n_f(\pi a\Phi R)\gamma\cos\theta. \tag{10}$$

Finally, Eq. (8) with Eq. (9) provides a complete prediction for the droplet trajectory with a single free parameter Φ.

IV. RESULTS

Initially, three-fiber arrays are discussed as they are the most basic array geometry that can capture a droplet in the inter-fiber volume. The fiber spacing is chosen such that confinement is small for 0.25 ml droplets $d \sim R$. Even with nylon fibers, only small amplitude $A < R$ fiber oscillations occur after droplet impact for the three-fiber arrays. Trajectories from Eq. (8), with unique optimum values of Φ, are plotted against measured z positions in Fig. 4. Droplet z positions are tracked from when the centroid is at the free end of the fiber array until the end of the drop tower test. A typical progression of a droplet into a fiber array is presented in Fig. 2. Droplet centroid locations are measured by fitting an ellipse to the droplet boundary. Predicted penetrations length agree well with experiments with an error between Eq. (8) at $t = 2.1$ and the measured penetration length ℓ_{stop}

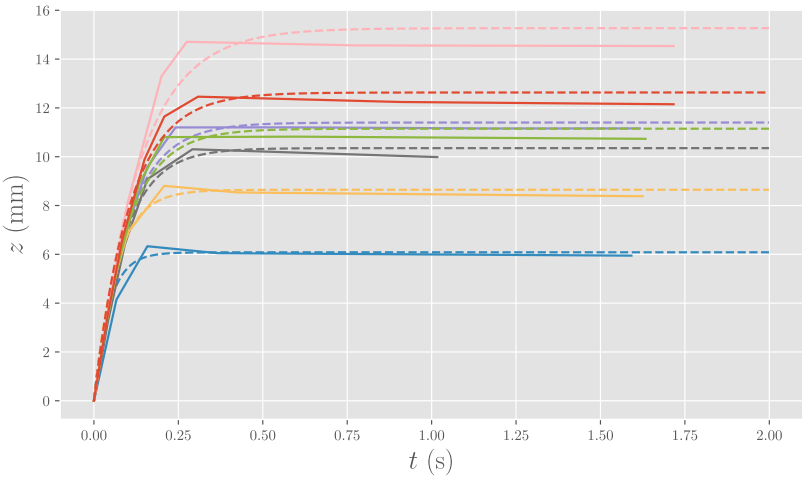

FIG. 4. Experimental measurements (solid) compared to equation Eq. (8) (dashed) with optimum values of Φ for 0.25ml droplet and three-fiber configurations. $F_{cl}/F_{\text{bulk}} \sim 300$ for these cases. Colors are to distinguish between individual drop tower tests.

of 8% on average. An average value $\Phi = 2.76$ is found for 0.25 ml droplets with a variance of 1.1. When using this average value of Φ the average error increases from 8% to 23%.

Letting $\Phi = 2.76$, the measured penetration length of all tests, with parameter ranges outlined in Table I, are compared to Eq. (8) at $t = 2.1$ in Fig. 5. The largest variation in behavior is for two-fiber arrays. This can be attributed to unpredictable behavior due the the lack of symmetry and confinement. The model tends to over-predict the penetration for droplet with volume greater than 0.25 ml. This overprediction is likely partially due to a larger contact line length caused by increased droplet confinement. For two-fiber arrays, the droplet is not constrained to any interfiber volume. For these tests, the droplet reaches an asymmetric equilibrium as a droplet attached to the side of both fibers, see Fig. 6(a). The most flexible fibers arranged in arrays of two fibers are shown to respond to drop impacts with large amplitude $A \sim R$ multi-mode fiber oscillations which are much larger than those observed for stainless steel fibers in an array of the same geometry, Fig. 6(b). For large amplitude oscillations, the contact length of the droplet grows and shrinks during each cycle. The contact line movement resulting from fiber oscillations was measured for various drops and found to be comparable to the penetration length. Therefore, the contact line dissipation associated with

TABLE I. The parameter regime explored in this experimental study of droplets impacting fiber arrays.

Parameter	Symbol	Range
Density	ρ	$1.0\,\mathrm{g\,cm^{-3}}$
Surface tension	γ	$72\,\mathrm{mN\,m^{-1}}$
Viscosity	μ	0.89 mPa s
Drop radius	R	3.6–7.8 mm
Drop jump velocity	v_j	$8.6–15.6\,\mathrm{cm\,s^{-1}}$
Number of fibers	n_f	2–13
Fiber length	L	22–73 mm
Fiber radius	a	0.1–0.8 mm
Fiber spacing	d	0.6–3.4 mm
Contact angle	θ	60°

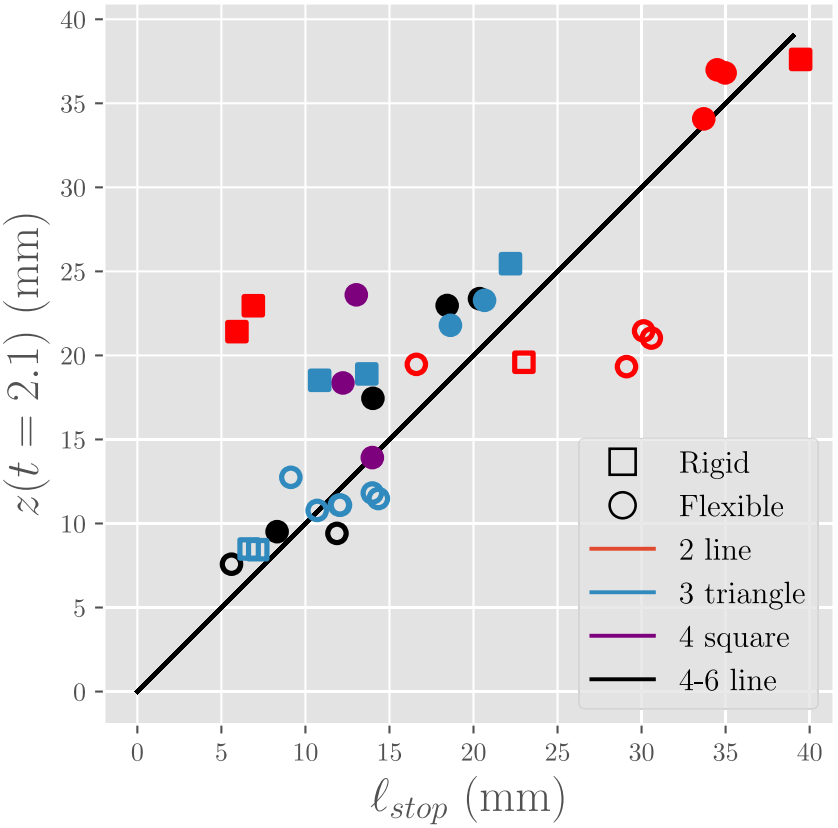

FIG. 5. Comparison between predicted and measured penetration length for a wide variety of fiber arrays with $\Phi = 2.76$. Open symbols are for 0.25 ml drops and filled symbols are for drops with 0.25 ml $<$ volume $\leqslant$ 1.0 ml.

the fiber oscillations is expected to play a significant role in reducing the final penetration length for the more flexible fibers.

For the fiber arrays in the line configuration, the fibers briefly pierced the droplet until the droplet migrated to one side of the fiber array. The force associated with the fiber piercing the droplet is assumed to be small for the limited number of small diameter fibers considered, and no significant deviation from the model is observed for these arrays. However, the model would have to be extended to capture the dynamics of penetration into fiber arrays, which have many fibers which continually pierce the droplet. The case of a fiber piercing an interface has been considered in Neukirch *et al.* [31] and Raufaste *et al.* [32]. A test of such a configuration is shown in Fig. 6(c). Further study of arrays with piercing fibers is left to future investigations.

V. DISCUSSION

A model based on dynamics which are dominated by viscous dissipation has been presented which can predict the penetration length of a droplet into a fiber array. By comparison with impact experiments performed in a drop tower, the model is shown to be robust over a wide range of parameters. Such a simple model has the advantage to capture the main findings of our experiments, indicating that viscous dissipation at the contact lines in particular controls the drop motion in the fibers array. A more complex model should take into account capillary terms and fiber elasticity in particular, and the complex geometry of the drop as it penetrates the fibers. It might improve

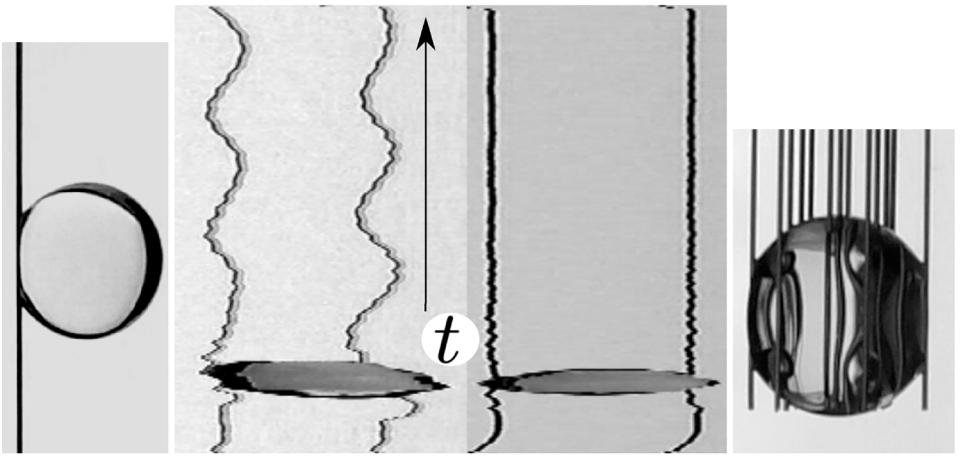

FIG. 6. (a) Asymmetric equilibrium configuration of a 0.5 ml droplet on a two-fiber array. (b) Kymograph (spatiotemporal diagrams) sampling the free end of the fiber showing fiber response to 0.25 ml droplet for flexible (left) and rigid (right) two-fiber arrays (c) Droplet equilibrium position in a hexagonal fiber array with six fibers on the droplet periphery and seven fibers piercing the droplet.

the quantitative comparisons with the experiments but at the cost of higher complexity, so that it is postponed to further investigations.

How the penetration length of a droplet in a fiber array can be altered by modifying the fiber properties and fiber arrangement is also studied here. It is shown that fibers which exhibit large amplitude oscillations reduce the penetration length relative to rigid fiber arrays of the same geometry. Additionally, this work presents a novel perspective on the static equilibrium configurations of fluid bodies in fiber arrays in the absence of gravity. For line configurations of fibers, the transition from a symmetric impact to an asymmetric equilibrium configuration as an off-center attached body is observed, see Fig. 6(a). The results of this work provide insight for applications such as fog harvesting, textile manufacturing, antisplash substrates, and microelectromechanical devices.

ACKNOWLEDGMENT

This work was supported by a NASA Space Technology Research Fellowship (NSTRF) under Grant No. 80NSSC19K1191.

[1] Q. Wang, X. Yao, H. Liu, D. Quéré, and L. Jiang, Self-removal of condensed water on the legs of water striders, Proc. Natl. Acad. Sci. **112**, 9247 (2015).

[2] H. G. Andrews, E. A. Eccles, W. C. E. Schofield, and J. P. S. Badyal, Three-dimensional hierarchical structures for fog harvesting, Langmuir **27**, 3798 (2011).

[3] A. A. Fedorets, E. Bormashenko, L. A. Dombrovsky, and M. Nosonovsky, Droplet clusters: Nature-inspired biological reactors and aerosols, Philos. Trans. R. Soc. A **377**, 20190121 (2019).

[4] M. Gürsoy, M. T. Harris, J. O. Downing, S. N. Barrientos-Palomo, A. Carletto, A. E. Yaprak, M. Karaman, and J. P. S. Badyal, Bioinspired fog capture and channel mechanism based on the arid climate plant salsola crassa, Colloids Surf., A **529**, 195 (2017).

[5] Z. Pan, W. G. Pitt, Y. Zhang, N. Wu, Y. Tao, and T. T. Truscott, The upside-down water collection system of syntrichia caninervis, Nature Plants **2**, 16076 (2016).

[6] W. Shi, M. J. Anderson, J. B. Tulkoff, B. S. Kennedy, and J. B. Boreyko, Fog harvesting with harps, ACS Appl. Mater. Interfaces **10**, 11979 (2018).
[7] B. Roman and J. Bico, Elasto-capillarity: Deforming an elastic structure with a liquid droplet, J. Phys.: Condens. Matter **22**, 493101 (2010).
[8] É. Lorenceau, C. Clanet, and D. Quéré, Capturing drops with a thin fiber, J. Colloid Interface Sci. **279**, 192 (2004).
[9] K. Piroird, C. Clanet, É. Lorenceau, and D. Quéré, Drops impacting inclined fibers, J. Colloid Interface Sci. **334**, 70 (2009).
[10] J. Comtet, B. Keshavarz, and J. W. M. Bush, Drop impact and capture on a thin flexible fiber, Soft Matter **12**, 149 (2016).
[11] E. Dressaire, A. Sauret, F. Boulogne, and H. A. Stone, Drop impact on a flexible fiber, Soft Matter **12**, 200 (2016).
[12] A. Nasto, P. T. Brun, and A. E. Hosoi, Drop impact on hairy surfaces, Phys. Rev. Fluids **4**, 064004 (2019).
[13] C. Duprat, S. Protière, A. Y. Beebe, and H. A. Stone, Wetting of flexible fibre arrays, Nature (London) **482**, 510 (2012).
[14] R. V. Dyba and B. Miller, Evaluation of wettability from capillary rise between filaments, Text. Res. J. **39**, 962 (1969).
[15] B. Miller, A. B. Coe, and P. Ramachandran, Liquid rise between filaments in a v-configuration, Text. Res. J. **37**, 919 (1967).
[16] F. W. Minor, A. M. Schwartz, E. Wulkow, and L. C. Buckles, The migration of liquids in textile assemblies: Part ii: the wicking of liquids in yams, Text. Res. J. **29**, 931 (1959).
[17] H. M. Princen, Capillary phenomena in assemblies of parallel cylinders, J. Colloid Interface Sci. **34**, 171 (1970).
[18] S. Protiere, C. Duprat, and H. A. Stone, Wetting on two parallel fibers: Drop to column transitions, Soft Matter **9**, 271 (2013).
[19] C. Py, R. Bastien, J. Bico, B. Roman, and A. Boudaoud, 3d aggregation of wet fibers, Europhys. Lett. **77**, 44005 (2007).
[20] J. Bico, B. Roman, and A. Boudaoud, Elastocapillary coalescence in wet hair, Nature (London) **432**, 690 (2004).
[21] É. Lorenceau and D. Quéré, Drops on a conical wire, J. Fluid Mech. **510**, 29 (2004).
[22] H. de Maleprade, M. Pautard, C. Clanet, and D. Quéré, Tightrope bubbles, Appl. Phys. Lett. **114**, 233704 (2019).
[23] A. P. Wollman, Capillarity-driven droplet ejection, Master's thesis, Portland State University, 2012.
[24] K. Cardin, S. Wang, O, Desjardins, M. Weislogel, Rebound of large jets from superhydrophobic surfaces in low gravity, Phys. Rev. Fluids **6**, 014003 (2021).
[25] S. Mora, T. Phou, J. M. Fromental, B. Audoly, and Y. Pomeau, Shape of an elastic loop strongly bent by surface tension: Experiments and comparison with theory, Phys. Rev. E **86**, 026119 (2012).
[26] B. Attari, M. Weislogel, A. Wollman, Y. Chen, and T. Snyder, Puddle jumping: Spontaneous ejection of large liquid droplets from hydrophobic surfaces during drop tower tests, Phys. Fluids **28**, 102104 (2016).
[27] J. Schindelin, I. Arganda-Carreras, E. Frise, V. Kaynig, M. Longair, T. Pietzsch, S. Preibisch, C. Rueden, S. Saalfeld, B. Schmid, J.-Y. Tinevez, D. J. White, V. Hartenstein, K. Eliceiri, P. Tomancak, and A. Cardona, Fiji: An open-source platform for biological-image analysis, Nature Methods **9**, 676 (2012).
[28] D. Bartolo, C. Josserand, and D. Bonn, Retraction dynamics of aqueous drops upon impact on non-wetting surfaces, J. Fluid Mech. **545**, 329 (2005).
[29] D. Bonn, J. Eggers, J. Indekeu, J. Meunier, and E. Rolley, Wetting and spreading, Rev. Mod. Phys. **81**, 739 (2009).
[30] P. G. de Gennes, Wetting: Statics and dynamics, Rev. Mod. Phys. **57**, 827 (1985).
[31] S. Neukirch, B. Roman, B. de Gaudemaris, and J. Bico, Piercing a liquid surface with an elastic rod: Buckling under capillary forces, J. Mech. Phys. Solids **55**, 1212 (2007).
[32] C. Raufaste, G. Kirstetter, F. Celestini, and S. J. Cox, Deformation of a free interface pierced by a tilted cylinder, Europhys. Lett. **99**, 24001 (2012).